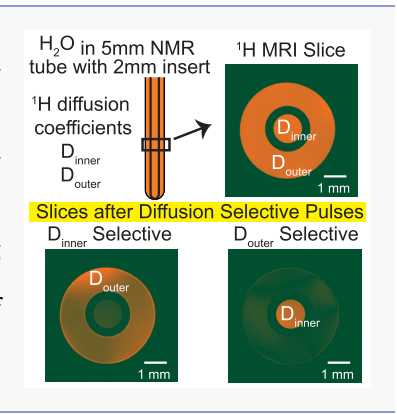
Diffusion Selective Pulses

Zhaoyuan Gong and Jamie D. Walls*

Department of Chemistry, University of Miami, Coral Gables, Florida 33146, United States

Supporting Information

ABSTRACT: The self-diffusion coefficient, D, provides important chemical and physical information about a molecular species and its environment, and D can be routinely measured under equilibrium conditions using nuclear magnetic resonance (NMR). Differences in diffusion coefficients can also be exploited in NMR to suppress signals from fast diffusing species relative to slow diffusing species. To date, no method for selectively suppressing signals only from species with a particular diffusion coefficient has been presented. In this work, diffusion selective pulses are developed that selectively suppress the magnetization only from species for which $D = D^{Sel}$. This is accomplished by interleaving NMR relaxation selective pulses between pulsed field gradients, where the effective transverse relaxation of the magnetization is related to D. Experimental demonstrations of diffusion selective pulses on water and water/acetone/dimethyl sulfoxide samples and on a magnetic resonance imaging phantom are presented.



easuring the apparent diffusion coefficient of a molecular species, D, can provide a lot of important chemical and physical information, such as its molecular size, its interactions with solvent and/or between other molecular species, its local environment, etc. It has long been appreciated that nuclear magnetic resonance (NMR) can be made sensitive to the effects of molecular diffusion by the application of pulsed field gradients (PFGs). Typically in NMR, D is determined by measuring the attenuation of the magnetization under PFGs in a Stejskal-Tanner experiment. For a collection of molecular species, diffusion-ordered spectroscopy or DOSY can be used to correlate self-diffusion coefficients to chemical shifts.2 As such, DOSY and its related variants have been invaluable tools in NMR mixture analysis, molecular binding and screening,4 chemical exchange,5 and a variety of other applications. Diffusion-diffusion correlation experiments have also been used to study exchange and aggregation.

Besides providing valuable physical and chemical information, differences in diffusion coefficients can also be exploited in NMR spectral editing. Diffusion-based spectral editing techniques have been used for solvent suppression,7 in addition to being used to highlight signals undergoing restricted diffusion.^{8,9} Essentially all of these diffusion-based spectral editing methods act like a "low-pass" filter, where signals from fast diffusing species for which $D \ge D^{Sel}$ are exponentially suppressed in an NMR spectrum relative to the signals from slow diffusion species for which $D \ll D^{\text{Sel}}$. However, this leads to the question of whether instead of a "low-pass" filter, a diffusion-based "notch filter" can be created that can selectively suppress the magnetization only from species for which $D = \hat{D}^{\text{Sel}}$.

In this Letter, we demonstrate that by combining PFGs with small flip-angle, radiofrequency (RF) pulses, a diffusion selective pulse that will suppress the magnetization only for those species for which $D = D^{Sel}$ can be generated. Such pulses could find applications for diffusion-based spectral editing in NMR and in magnetic resonance imaging (MRI). Diffusion selective pulses work by taking advantage of the fact that diffusion in the presence of magnetic field gradients results in an effective transverse or T_2 relaxation of the magnetization that is related to D. 10 As such, relaxation selective pulses 11-14 that suppress the magnetization for those spins with a particular set of T_2 and longitudinal (T_1) relaxation times can be interwoven between PFG blocks to selectively suppress the magnetization from species for which $T_2 = T_2^{\text{Sel}}$ and hence

Consider the magnetization from a collection of $N_{\rm sp}$, $I = \frac{1}{2}$ spins with gyromagnetic ratio γ in the presence of a large, static magnetic field oriented along the \hat{z} -direction, $\vec{B}_0 = B_0 \hat{z}$. In this case, the thermal equilibrium magnetization at temperature Tis aligned along \vec{B}_0 , $\vec{M}_{eq} = M_{eq}\hat{z}$, where $M_{
m eq}=\hbar\gamma N_{
m sp}\; {
m tanh}igg(rac{\hbar\omega_0}{2k_{
m B}T}igg)$ represents the magnitude of the total equilibrium magnetization, $\omega_0 = \gamma B_0$ is the Larmor frequency, and $k_{\rm B}$ is the Boltzmann constant. When the magnetization is perturbed from equilibrium, for example, because of the application of an RF pulse, the time evolution of the total magnetization, $\vec{M}(t) = M_X(t)\hat{x} + M_Y(t)\hat{y} + M_Z(t)\hat{z}$, is governed by the Bloch equations:

Received: October 31, 2019 Accepted: December 26, 2019 Published: December 26, 2019



The Journal of Physical Chemistry Letters

$$\frac{\mathrm{d}}{\mathrm{d}t} \begin{pmatrix} M_{\mathrm{eq}} \\ M_Z(t) \\ M_+(t) \\ M_-(t) \end{pmatrix} = \left[\hat{\mathcal{L}}_0(T_1, T_2, \omega_{\mathrm{off}}) + \hat{H}_{\mathrm{RF}}(\omega_{\mathrm{RF}}(t), \phi(t)) \right] \begin{pmatrix} M_{\mathrm{eq}} \\ M_Z(t) \\ M_+(t) \\ M_-(t) \end{pmatrix}$$
(1)

where $M_{\pm}(t) = M_X(t) \pm i M_Y(t)$, $\hat{H}_{RF}(\omega_{RF}(t), \phi(t))$ is the superoperator¹⁵ representing an RF pulse of amplitude $\omega_{RF}(t)$ and phase $\varphi(t)$, and

$$\hat{\mathcal{L}}_{0}(T_{1}, T_{2}, \omega_{\text{off}}) = \begin{pmatrix}
0 & 0 & 0 & 0 \\
\frac{1}{T_{1}} - \frac{1}{T_{1}} & 0 & 0 \\
0 & 0 & -\frac{1}{T_{2}} - i\omega_{\text{off}} & 0 \\
0 & 0 & 0 & -\frac{1}{T_{2}} + i\omega_{\text{off}}
\end{pmatrix} \tag{2}$$

represents the intrinsic Liouvillian superoperator in the absence of RF irradiation, where $\omega_{\rm off}$ is the I spin resonance frequency in the rotating frame, and $(T_1)^{-1}$ and $(T_2)^{-1}$ are the intrinsic longitudinal and transverse magnetization relaxation rates, respectively, for the magnetization to evolve back to $\vec{M}_{\rm eq}$. The formal solution to eq 1 is given by

$$\begin{pmatrix} M_{\rm eq} \\ M_Z(t) \\ M_+(t) \\ M_-(t) \end{pmatrix} = \hat{\mathcal{R}}_0((\omega_{\rm RF})_\phi, t, 0) \begin{pmatrix} M_{\rm eq} \\ M_Z(0) \\ M_+(0) \\ M_-(0) \end{pmatrix}$$
(3)

where $\hat{\mathcal{R}}_0((\omega_{\mathrm{RF}})_\phi,\,t,\,0)=\hat{T}\,\mathrm{e}^{\int_0^t\mathrm{d}t'(\hat{\mathcal{L}}_0(T_1,T_2,\omega_{\mathrm{off}})+\hat{H}_{\mathrm{RF}}(\omega_{\mathrm{RF}}(t\,\prime),\varphi(t\,\prime)))}$ is time evolution propagator with \hat{T} being the Dyson time-ordering operator.

The dynamics of the magnetization in eq 1 can be sensitized to molecular diffusion by the application of PFGs. Consider the sequence shown in Figure 1A, which is composed of two gradient recalled echoes (GREs) that form a GRE block. When taking into account the effects of molecular diffusion during the sequence in Figure 1A, the net effect is for $\vec{M}(t)$ to evolve for a time $\tau_c = 2(\Delta + \delta + 2t_d)$ into

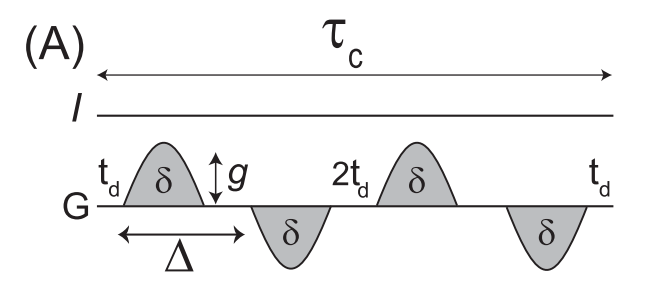
$$M_{\pm}(t+\tau_{c}) = \exp\left(-\left[\frac{1}{T_{2}^{\text{Eff.}}} \pm i\omega_{\text{off}}\right]\tau_{c}\right)M_{\pm}(t)$$

$$M_{Z}(t+\tau_{c}) = M_{\text{eq}} + (M_{Z}(t) - M_{\text{eq}})\exp\left(-\frac{\tau_{c}}{T_{1}}\right)$$
(4)

In eq 4, $T_2^{\text{Eff.}}$ is the effective transverse relaxation time during the GRE block, which is given by

$$\frac{1}{T_2^{\text{Eff.}}} = \frac{1}{T_2} + \frac{2D_{\text{I}}(\gamma g f_1 \delta)^2 (\Delta - f_2 \delta)}{\tau_c}$$

$$\approx \frac{2D_{\text{I}}(\gamma g f_1 \delta)^2 (\Delta - f_2 \delta)}{\tau_c}$$
(5)



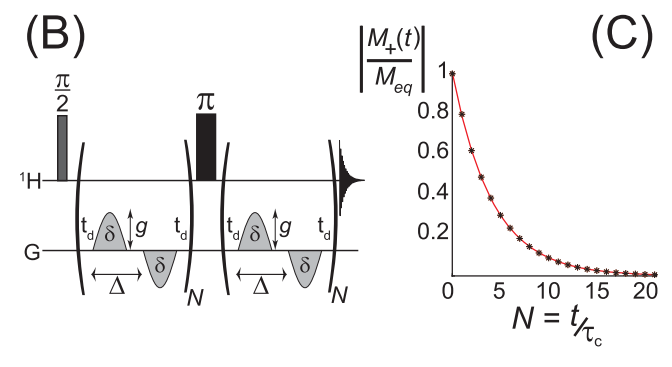


Figure 1. Sensitizing the magnetization dynamics to the self-diffusion coefficient using PFGs. (A) Basic gradient-recalled echo (GRE) block to "sensitize" the transverse magnetization to molecular diffusion, where g and δ are the maximum gradient strength and length of an individual pulsed field gradient (PFG), respectively, where $\tau_c = 2(\Delta + \delta + 2t_d)$. (B) Spin echo experiment to measure $T_2^{\rm Eff.}$ under a series of GRE blocks. (C) Experimental data (black asterisks) and the corresponding fit (red solid curve) to eq 4 for $M_+(N\tau_c)$ in a 1:1 (v/v) H_2O/D_2O solution with $T_{2,H_2O}^{\rm Obs.} = 97.83 \pm 0.67$ ms, which was close to $T_{2,H_2O}^{\rm Eff.} = 94$ ms calculated using eq 5 with $\Delta = 6$ ms, $\delta = 5$ ms, $t_d = 400~\mu s$, g = 12.81~G/cm, and the experimentally measured D_{H_2O} and T_{2,H_2O} values listed in Table 1.

where $D_{\rm I}$ (square centimeters per second) is the self-diffusion coefficient, g (gauss per centimeter) and δ (seconds) are the maximum strength and length of the PFG, respectively, Δ (seconds) is the diffusion delay, and $f_{\rm 1}$ and $f_{\rm 2}$ are dimensionless parameters that depend on the PFG's shape ¹⁶ (for example, $f_{\rm 1}=\frac{2}{\pi}$ and $f_{\rm 2}=\frac{1}{4}$ for sine-shaped PFGs, which were used in this work). The last approximation in eq 5 is valid only under conditions when the transverse relaxation is completely dominated by diffusion during the GRE block, which can be a good approximation for large enough values of g and δ .

In this case, the evolution over a GRE block described in eq 4 is equivalent to a system undergoing regular "free evolution" under \mathcal{L}_0 in eq 2 but with T_2 replaced by $T_2^{\text{Eff.}}$ in eq 5, i.e., $\hat{\mathcal{L}}_{\text{GRE}} \equiv \hat{\mathcal{L}}_0(T_1, T_2^{\text{Eff.}}, \omega_{\text{off}})$. To demonstrate that the decay rate of the transverse magnetization under GRE blocks is indeed given by $(T_2^{\text{Eff.}})^{-1}$ from eq 5, the effective ¹H transverse relaxation of a 1:1 (v/v) $H_2\text{O}/D_2\text{O}$ sample under GRE blocks with g=12.81 G/cm, $\delta=5$ ms, $\Delta=6$ ms, and $t_d=400~\mu\text{s}$ was measured using the spin echo sequence shown in Figure 1B, where a π -pulse was used to partially refocus sample field inhomogeneity (for example, because of imperfect magnetic shimming) prior to acquisition. Fitting the decay of the transverse magnetization to eq 4 gave an observed transverse relaxation time under the GRE blocks, T_{2,H_2O}^{Obs} , of 97.83 \pm 0.67 ms as shown in Figure 1C, which was close to the theoretical $T_2^{\text{Eff.}}$ value of 94 ms calculated using eq 5.

As suggested by eq 5 and Figure 1C, differences in $D_{\rm I}$, and hence differences in $T_2^{\text{Eff.}}$, could be exploited to selectively suppress signals using relaxation selective pulses. Relaxation selective pulses are RF pulses that selectively suppress the magnetization for species with relaxation times given by T_1 = T_1^{Sel} and $T_2 = T_2^{\text{Sel}}$. Relaxation selective pulses typically work by both inverting the initial equilibrium magnetization, $M_{\rm eq}$, and attenuating it by an amount related to both T_2 and T_1 . Once inverted, the magnetization undergoes T_1 relaxation back to $\vec{M}_{\rm eq}$ with the magnetization being nulled at the end of a relaxation selective pulse of length $T_{\rm p}$ for those species for which $T_1 = T_1^{\rm Sel}$ and $T_2 = T_2^{\rm Sel}$. Typically species for which $T_2 < T_2^{\rm Sel}$ $T_2^{\rm Sel}$ exhibit greater magnetization attenuation compared to spins for which $T_2=T_2^{\rm Sel}$ prior to the inversion recovery period and thus end up with \hat{z} -magnetization oriented along the $+\hat{z}$ direction, whereas species for which $T_2 > T_2^{\text{Sel}}$ typically experience less magnetization attenuation prior to the inversion recovery period and thus end up with \hat{z} -magnetization oriented along the $-\hat{z}$ -direction. The diffusion selective pulses used in this work utilize a combination of T_1 and effective T_2 relaxation to suppress signals based upon $D_{\rm I}$. It should be noted that most relaxation selective pulses use lowpower RF strengths that make them sensitive to B_0 inhomogeneity and RF transmitter offsets (more details of the mechanisms of relaxation selective pulses are given in the Supporting Information).

Before going on to discuss how to generate diffusion selective pulses from relaxation selective pulses, we should consider the case in which T_1 relaxation can be safely ignored, i.e., $T_1 \gg T_2$. This situation can in principle be achieved due to diffusion under PFGs as long as sufficiently strong gradient strengths are used (technical limitations on gradient strengths and the time it takes to switch such strong gradients on and off while minimizing eddy currents may make it challenging to completely ignore T_1 relaxation in diffusion selective pulses). However, the mechanism behind T_2 relaxation selective pulses 11,12 is slightly different than that of the relaxation selective pulses described above. In this case, the overall magnetization of spins for which $T_2 \neq T_2^{\text{Sel}}$ is attenuated under the T_2 -selective pulse, while those spins for which $T_2 > T_2^{\rm Sel}$ have their magnetization inverted to point along the $-\hat{z}$ -direction. For $T_2 = T_2^{\text{Sel}}$, the T_2 -selective pulses simply rotate \vec{M}_{eq} by $\Theta = \frac{\pi^2}{2}$ into the x-y plane while exponentially attenuating the magnetization. The theoretical attenuation of the total magnetization after application of a T_2 -selective pulse

as a function of
$$T_2$$
, $\left| \frac{\vec{M}(T_2)}{M_{eq}} \right|$, is given by 12

$$\left| \frac{\vec{M}(T_2)}{M_{\text{eq}}} \right| = \left| \frac{T_2 - T_2^{\text{Sel}}}{T_2 + T_2^{\text{Sel}}} \right|$$

$$\approx \left| \frac{D_I - D^{\text{Sel}}}{D_I + D^{\text{Sel}}} \right|$$
(6)

where the approximation in the last line of eq 6 is valid only when $T_2^{\text{Eff.}}$ is mainly determined by D_1 in eq 5. A plot of $\left|\frac{\vec{M}(T_2^{\text{Eff.}})}{M_{\text{eq}}}\right|$ versus $T_2^{\text{Eff.}}$ is given in Figure 2C (solid black curve).

Any relaxation selective pulse that selectively suppresses the magnetization for spins with $T_2 = T_{2,\mathrm{I}}^{\mathrm{Eff.}}(D^{\mathrm{Sel}}) = \frac{\tau_{\mathrm{c}}}{2D^{\mathrm{Sel}}(\gamma g f, \delta)^2 (\Delta - f, \delta)} \quad \text{will therefore act, by}$

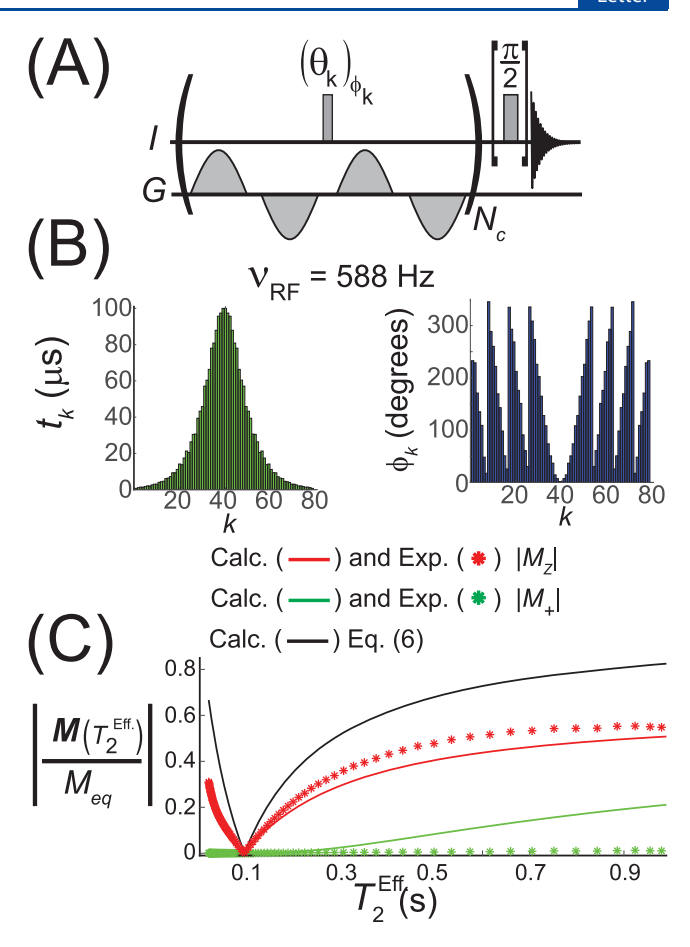


Figure 2. Basic scheme for implementing a diffusion selective pulse and an experimental demonstration of a diffusion selective pulse in a 1:1 (v/v) H₂O/D₂O sample. (A) A series of N_c GRE blocks from Figure 1A with an RF pulse of fixed amplitude $\nu_{\rm RF}$ placed in the middle of each GRE block with phase φ_k and flip angle $\theta_k = 2\pi\nu_{RE}t_k$ for k = 1 to $k = N_c$. The resulting \hat{z} -magnetization/transverse magnetization after application of the diffusion selective pulse can be measured with or without application of a $\frac{\pi}{2}$ pulse prior to signal acquisition. (B) Pulse lengths, $0 < t_k \le 100 \ \mu s$ and phases, φ_k , for k =1 to $k = N_c = 78$ pulses used to generate a diffusion selective pulse that suppresses the magnetization from spins with $T_2^{\text{Sel}} \approx 94$ ms. (C) Experimental profiles of the longitudinal (red asterisks) and transverse magnetization (green asterisks) after application of the diffusion selective pulse in panel B to a 1:1 (v/v) H_2O/D_2O sample as a function of $T_{2,H,O}^{Eff.}$ (calculated using eq 5). The corresponding magnetization profiles (solid red and green curves) calculated using eq 1 are shown along with (solid black curve) the theoretical magnetization profile for a T_2 -selective pulse in eq 6. A minimum in $|M(T_{\rm p})|$ occurred near $T_2^{\rm Sel}$ = 97 ms. In the GRE blocks, Δ = 6 ms, δ = 5 ms, $t_{\rm d}$ = 400 μ s, $\tau_{\rm c}$ = 23.6 ms, and $T_{\rm p}$ = $N_{\rm c}\tau_{\rm c}$ = 1.8408 s, and g was linearly varied from 0.298 to 29.8 G/cm.

default, as a diffusion selective pulse that also suppresses the magnetization for those species for which $D_{\rm I}=D^{\rm Sel}$. However, because $T_{\rm 2,I}^{\rm Eff.}$ in eq 5 is the effective transverse relaxation time over a GRE block, RF pulses must be applied in such a way that, when averaged over a GRE block, they generate an evolution of the magnetization that is equivalent to the evolution generated by applying a relaxation selective pulse to a system with a Liouvillian given by $\hat{\mathcal{L}}_{\rm GRE}$. This can be accomplished as follows.

Consider a relaxation selective pulse with amplitude and phase given by $\omega^{\rm Sel}(t)$ and $\varphi^{\rm Sel}(t)$ for $0 \le t \le T_{\rm p}$ that is

Table 1. Experimentally Determined Spectral Parameters at a Field Strength of 400 MHz

sample	species	δ (ppm)	$D \ (\times 10^{-6} \ \text{cm}^2 \ \text{s})$	T_1 (s)	T_2 (s)
Figures 1 and 2, 1:1 (v/v) H ₂ O/D ₂ O	H_2O	4.7	19.99 ± 0.40	7.44 ± 0.06	1.01 ± 0.03
Figure 3, 1:1:1:3 (v/v/v/v) DMSO/acetone/H ₂ O/D ₂ O	H_2O	4.7	11.49 ± 0.16	4.21 ± 0.11	2.37 ± 0.06
	DMSO	2.72	6.16 ± 0.08	3.35 ± 0.05	3.22 ± 0.05
	acetone	2.23	7.43 ± 0.01	5.53 ± 0.43	5.47 ± 0.13
Figure 4, outer tube, 1:1 (v/v) H_2O/D_2O , $[Gd^{3+}] = 88 \mu M$	H_2O	4.7	21.01 ± 0.01	0.59 ± 0.04	0.38 ± 0.01
Figure 4, inner tube, 1:1 (v/v) $H_2O/DMSO-d_6$, pH 4.56	H_2O	4.7	7.52 ± 0.34	1.20 ± 0.01	0.71 ± 0.02

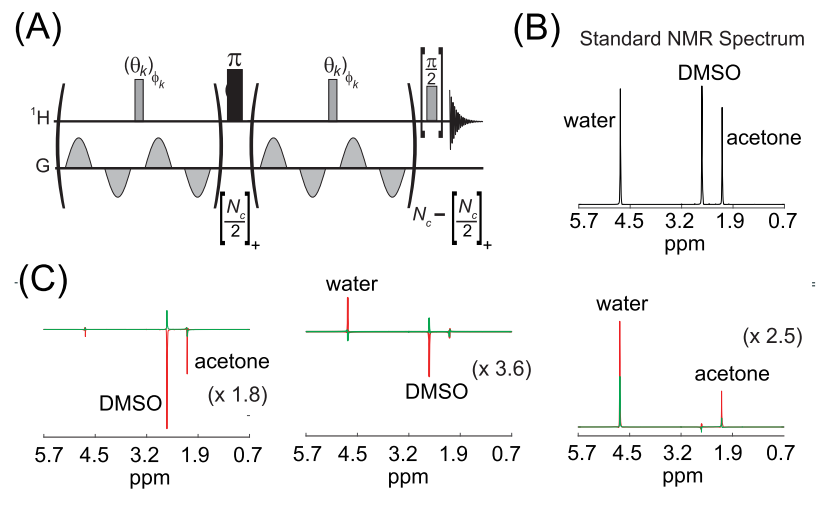


Figure 3. Using diffusion selective pulses to suppress signals based upon the self-diffusion coefficients in a 1:1:1:3 (v/v/v/v) DMSO/acetone/ H_2O/D_2O solution. (A) Application of a diffusion selective pulse with a π -pulse placed roughly in the middle ($[z]_+$ = ceiling of z). In all experiments, g = 44.7 G/cm, $\delta = 3$ ms, $\Delta = 4$ ms, $t_d = 400$ μ s, $\tau_c = 15.6$ ms, and the RF transmitter was placed at the average frequency offset ($\delta_{transmitter} = 3.22$ ppm). (C) Corresponding spectra from the resulting transverse (green) and \hat{z} -magnetization (red) after application of diffusion selective pulses designed to suppress the water (left), acetone (middle), or DMSO (right) resonances. Scaling factors relative to the regular NMR spectrum in panel B are shown. Details of the diffusion selective pulses and spectral integrals are given in the Supporting Information.

designed to suppress the magnetization of spins for which $T_2^{\rm Sel}$ = $T_2^{\rm Eff}(D_1^{\rm Sel})$. Furthermore, suppose that the relaxation pulse can be approximated by $N_{\rm c}$ rectangular pulses, each of length $\tau_{\rm c}$ for which $T_{\rm p} \approx N_{\rm c}\tau_{\rm c}$ and with the phase and amplitude of the kth pulse for k=1 to $k=N_{\rm c}$ given by $\varphi_k^{\rm Sel}$ and $\varphi_k^{\rm Sel}$ and into a diffusion selective pulse using the pulse sequence in Figure 2A, which consists of $N_{\rm c}$ GRE blocks with an RF pulse of fixed amplitude $\nu_{\rm RF}$ applied in the middle of the GRE block. The phase and flip angle of the kth RF pulse of length $0 \le t_k \le 2t_{\rm d}$ in Figure 2A are given by $\varphi_k^{\rm Sel}$ and $\theta_k = 2\pi\nu_{\rm RF}t_k \equiv \omega_k^{\rm Sel}\tau_{\rm c}$ respectively, for k=1 to $k=N_{\rm c}$. Due to the RF pulse, the evolution during the kth GRE block for k=1 to $k=N_{\rm c}$ can be described by an average Liouvillian 17 given by

$$\overline{\mathcal{L}}_{\text{GRE}}^{k} \approx \hat{\mathcal{L}}_{\text{GRE}} + \hat{H}_{\text{RF}} \left(\frac{t_{k}}{\tau_{c}} 2\pi \nu_{\text{RF}}, \, \phi_{k}^{\text{Sel}} \right)$$

$$= \hat{\mathcal{L}}_{\text{GRE}} + \hat{H}_{\text{RF}} (\omega_{k}^{\text{Sel}}, \, \phi_{k}^{\text{Sel}}) \tag{7}$$

Equation 7 is valid 18 as long as $\omega_k t_k \ll \frac{\pi}{3}$ and $|\omega_1 \tau_c| \ll \frac{\pi}{3}.$

The overall propagator for the $N_{\rm c}$ GRE blocks in Figure 2 can therefore be written as

$$\hat{\mathcal{R}}^{\mathrm{DSP}}(T_{\mathrm{p}}) \approx \hat{T} \prod_{k=1}^{N_{\mathrm{c}}} e^{\tau_{\mathrm{c}} [\hat{\mathcal{L}}_{\mathrm{GRE}} + \hat{H}_{\mathrm{RF}}(\omega_{k}^{\mathrm{Sel}}, \phi_{k}^{\mathrm{Sel}})]}$$

$$\approx \hat{T} e^{\int_{0}^{T_{\mathrm{p}}} \mathrm{d}t' [\hat{\mathcal{L}}_{\mathrm{GRE}} + \hat{H}_{\mathrm{RF}}(\omega^{\mathrm{Sel}}(t_{\ell}), \phi^{\mathrm{Sel}}(t_{\ell}))]}$$
(8)

where the superscript DSP stands for diffusion selective pulse. Equation 8 represents the total propagator for the application of a relaxation selective pulse of length $T_{\rm p}$ and with amplitude $\omega^{\rm Sel}(t)$ and phase $\varphi^{\rm Sel}(t)$ applied to a system with a Liouvillian given by $\hat{\mathcal{L}}_{\rm GRE}$. The diffusion selectivity of the sequence in Figure 2A comes from the diffusion dependence of $T_2^{\rm Eff.}$ in eq 5.

A demonstration of a diffusion selective pulse applied to a 1:1 (v/v) H_2O/D_2O sample is given in Figure 2. In Figure 2B, the pulse lengths, $0 < t_k \le 100~\mu s$, and phases, φ_k for k=1 to $k=N_c=78$ that were used in Figure 2A to generate a frequency-swept hyperbolic secant ¹⁹-based relaxation selective pulse for which $T_2^{\rm Sel}=94$ ms and $T_p=N_c\tau_c=1.8408$ s are shown. While frequency-swept hyperbolic secant pulses are relatively robust to RF inhomogeneity, the diffusion selective pulse in Figure 2B, and as implemented in Figure 2A, was very sensitive to B_0 inhomogeneity and RF transmitter offset.

The attenuation of the magnetization under the diffusion selective pulse in Figure 2B versus $T_2^{\rm Eff.}$ is shown in Figure 2C. In this case, different values of $T_2^{\rm Eff.}$ were generated by linearly varying the PFG gradient strength from g=0.298 G/cm (corresponding to $T_2^{\rm Eff.}=995$ ms as calculated from eq 5) to g=29.8 G/cm (corresponding to $T_2^{\rm Eff.}=19$ ms). For each g, and hence for each $T_2^{\rm Eff.}$, both the total transverse (green) and the total \hat{z} -magnetization (red) after application of a diffusion selective pulse were measured by integrating the resulting spectrum about the water resonance over a ± 3 Hz range. In Figure 2C, the experimentally measured integrals (normalized by the integral from a regular spectrum) are represented by an asterisk while the solid red and green curves represent the

theoretical predictions based on numerically integrating eq 1 for the pulse sequence shown in Figure 2A. The theoretical attenuation curve for a purely T_2 -selective pulse for which $T_2^{\rm Sel}=94$ ms, calculated using eq 6, is also shown (solid black curve). As shown in Figure 2C, the total magnetization was suppressed at $T_{2,{\rm H}_2{\rm O}}^{\rm Eff.}\approx 97$ ms with observed transverse and \hat{z} -magnetization of $|M_+|\approx 3.1\times 10^{-4}M_{\rm eq}$ and $|M_Z|\approx 3.5\times 10^{-3}M_{\rm eq'}$ respectively. Note that for $T_{2,{\rm H}}^{\rm Eff.}>97$ ms, the \hat{z} -magnetization was inverted as expected (data not shown).

Diffusion selective pulses were also developed to selectively suppress signals in a 1:1:1:3 (v/v/v/v) DMSO/acetone/H₂O/ D₂O sample (spectral parameters are listed in Table 1 with the regular NMR spectrum given in Figure 3B). In these experiments, GRE blocks using g = 44.7 G/cm, $\delta = 3$ ms, Δ = 4 ms, $t_{\rm d}$ = 400 μ s, and $\tau_{\rm c}$ = 15.6 ms were used, which gave effective $T_2^{\text{Eff.}}$ values of $T_{2,\text{H,O}}^{\text{Eff.}} = 37.1$ ms, $T_{2,\text{acetone}}^{\text{Eff.}} = 58.3$ ms, and $T_{2,{\rm DMSO}}^{\rm Eff.}$ = 71.2 ms under these conditions. In this case, diffusion selective pulses were optimized using a modified version of the GRAPE algorithm²⁰ applied to the sequence in Figure 3A where a π -pulse was placed in the approximate middle of the diffusion selective pulse to help refocus chemical shifts before signal acquisition (details of the optimization, the corresponding diffusion selective pulses, and integrals of the spectra in Figure 3C after application of the diffusion selective pulses can be found in the Supporting Information). In each case, a soliton T_2 -selective pulse for suppressing the relevant $T_2^{
m Eff.}$ was used as initial input into the optimization algorithm.

In Figure 3C, the resulting spectra from the remaining transverse (green) and \hat{z} -magnetization (red) after application of diffusion selective pulses that were designed to selectively suppress signals from H₂O (Figure 3C, left), acetone (Figure 3C, middle), and DMSO (Figure 3C, right) are shown. In Figure 3C, the diffusion selective pulses suppressed signals with the corresponding $T_2^{\rm Eff.} = T_2^{\rm Sel}$ while inverting the signals for those species for which $T_2^{\rm Eff.} > T_2^{\rm Sel}$.

Finally, diffusion selective pulses were applied on a sample of water in two different, spatially separated chemical environments with distinct diffusion coefficients. The sample consisted of a 5 mm NMR tube with a 2 mm coaxial insert with an 88 μ M Gd³⁺, 1:1 (v/v) H₂O/D₂O solution in the "outer compartment" and a 1:1 (v/v) H₂O/DMSO-d₆ solution at pH 4.56 in the "inner compartment" (see the inset in Figure 4A). Although the two solutions were spatially separated, the chemical shifts and ratios of $\frac{T_1}{T_2}$ in the two compartments were similar enough that the regular sample spectrum in Figure 4A consisted of a single resonance with $\Delta \nu_{1/2} = 12$ Hz. However, the self-diffusion coefficient in the "outer compartment" was a factor of ~3 larger than that found in the "inner compartment" (Table 1). In Figure 4B, a proton density image from a 1 mm slice shows the signals from the two compartments. Using GRE blocks with g = 23.92 G/cm, $\tau_c = 18.45$ ms, $\delta = 3$ ms, $\Delta =$ 5.11 ms, and $t_{\rm d}$ = 500 μ s, the effective transverse relaxation times were $T_{2,\text{outer}}^{\text{Eff.}} = 69.35 \text{ ms}$ and $T_{2,\text{inner}}^{\text{Eff.}} = 158.6 \text{ ms}$ in the outer and inner tubes, respectively, which agreed well with the theoretical values of $T_{2,\text{outer}}^{\text{Eff.}} = 65.0 \text{ ms}$ and $T_{2,\text{inner}}^{\text{Eff.}} = 158.4 \text{ ms}$ calculated from eq 5. Under these conditions, images were taken after application of diffusion selective pulses designed to selectively suppress signals in either the outer compartment (Figure 4D; $T_p = 313.65$ ms) or the inner compartment (Figure 4C; $T_p = 793.35$ ms). As demonstrated in Figure 4,

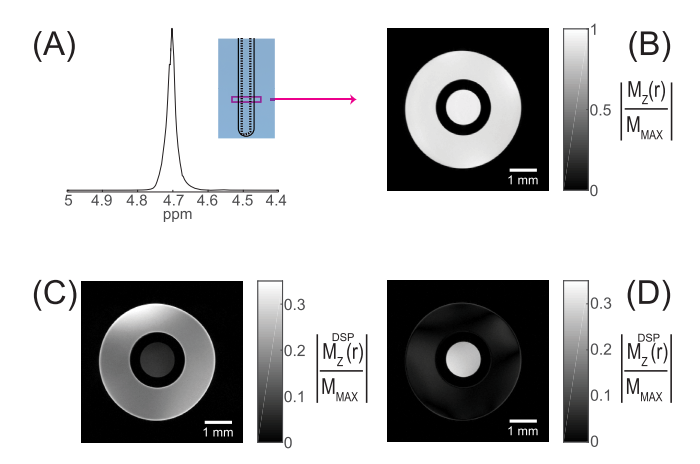


Figure 4. Application of diffusion selective pulses to spatially suppress signals based upon differences in self-diffusion coefficients. (A) A 5 mm NMR tube with a 2 mm coaxial insert was used (see the inset) with an 88 μ M Gd³⁺ solution in a 1:1 (v/v) H₂O/D₂O solution in the outer compartment and a pH 4.56, 1:1 (v/v) H₂O/DMSO-d₆ solution in the inner compartment. The spectrum consisted of a relatively broad beak with a line width $(\Delta \nu_{1/2})$ of 12 Hz. (B) FLASH image representing a 1 mm slice in the x-y plane of the sample that clearly shows the two sample regions (inner and outer tubes), which have nearly the same proton density in both regions. Using GRE blocks with g = 23.92 G/cm, $\tau_c = 18.45$ ms, $\delta = 3$ ms, $\Delta = 5.11$ ms, and t_d = 500 μ s, diffusion selective pulses were designed to suppress signals in the inner compartment (panel C; $T_{2,\text{inner}}^{\text{Eff.}} = 158.6 \text{ ms}$) or the outer compartment (panel D; $T_{2,\text{outer}}^{\text{Eff.}} = 69.35 \text{ ms}$). The same slice as in panel B was acquired after application of a diffusion selective pulse designed to suppress either the (C) slow diffusing species (inner compartment) or the (D) fast diffusing species (outer compartment).

diffusion selective pulses can be used to spatially differentiate signals based upon self-diffusion coefficients.

In summary, we have presented a new method for selectively suppressing signals in an NMR experiment based upon the self-diffusion coefficient, D. This was accomplished by exploiting the fact that PFGs can sensitize the effective transverse magnetization relaxation time to D as given in eq 5. As a result, diffusion selective pulses can be constructed by incorporating T_2 -selective pulses into a series of PFG blocks. Experimental demonstrations in both water and DMSO/ acetone/water samples were presented that illustrated the capabilities of diffusion selective pulses to selectively suppress signals based upon D for both spectroscopic and imaging applications. Diffusion selective pulses provide a new experimental control for editing and acquiring NMR spectra. In addition, diffusion selective pulses may find use in multidimensional diffusion experiments, 21 in suppressing background signals from immobile fats in MRI, and in quantifying distributions of diffusion coefficients in multicomponent samples to name just a few potential applications. Finally, the performance of the diffusion selective pulses presented in this work can be significantly improved by developing better optimization algorithms that could make the pulses more robust to chemical shifts, spin-spin couplings, etc. In addition, both PFG and RF shapes could be simultaneously optimized to generate diffusion selective pulses that are robust to RF and B_0 inhomogeneity while minimizing the attenuation of magnetization for species for which $D \neq D^{Sel}$.

■ EXPERIMENTAL SECTION

Acetone (99.5% pure), dimethyl sulfoxide (DMSO, 99.5% pure), and gadolinium(III) chloride hexahydrate (99.999% pure) were purchased from Sigma-Aldrich. Hydrochloric acid (HCl, 6 N) was purchased from VWR International, and D_2O (D, 99.9%) and DMSO- d_6 (D, 99.9%) were purchased from Cambridge Isotope Laboratories, Inc. All experiments were carried out on a 400 MHz Bruker AVANCE III HD spectrometer with a MicroS microimaging probe equipped with *XYZ* gradients and only a 1 H channel. The self-diffusion coefficients were measured using pulsed gradient stimulated echo (PGSTE) experiments, and the longitudinal and transverse relaxation times were determined using inversion recovery and CPMG^{23,24} (with a π -pulse spacing of 200 ms) experiments, respectively.

All diffusion selective pulses were implemented using sine-shaped PFGs. For applications of the sequences in Figures 2A and 4A, the directions of the PFGs in different GRE blocks were randomized within an experiment to minimize the contributions of stimulated echoes and eddy currents so that acquisition of the free induction decay (FID) could begin at approximately at the end of the last GRE block. If only a Z-gradient was available, randomizing between $\pm Z$ PFGs within an experiment was also found to reduce the contributions of stimulated echoes to the FID. All spectra were acquired using a dwell time of $\Delta t = 250~\mu s$, $N_{\rm pts} = 4799$ complex data points, eight scans, and a relaxation delay (d_1) of either 40 s (Figures 2 and 3) or 7 s (Figure 4).

For the imaging experiments in Figure 4, a 5 mm NMR tube (Wilmad LabGlass, 528-PP-7CONS) containing an 88 μ M Gd³+ solution in a 1:1 (v/v) H₂O/D₂O mixture with a 2 mm coaxial inert (Wilmad LabGlass, WGS-5BL) that contained a 1:1 (v/v) H₂O/DMSO- d_6 solution with a calculated pH of 4.56 was used. Under the shimming condition of this probe, the difference in resonance frequencies between the two solutions was <3 Hz with the overall spectrum in Figure 4A having a line width at half-height ($\Delta\nu_{1/2}$) of 12 Hz. After application of the diffusion selective pulses (which are given in the Supporting Information), images were acquired using a standard FLASH²-5 sequence with an echo time of TE = 3.663 ms, a repetition time of TR = 7 s, one signal average, an excitation flip angle of $\Theta = \frac{\pi}{2}$, a 1 mm axial slice, and a 256 × 256 image size with a field of view of 6 mm × 6 mm.

ASSOCIATED CONTENT

Supporting Information

The Supporting Information is available free of charge at https://pubs.acs.org/doi/10.1021/acs.jpclett.9b03222.

Additional details about the theory presented in this work, the mechanisms of relaxation selective pulses, the various diffusion selective pulse shapes, and a basic description of the modifications to the gradient ascent pulse engineering or GRAPE algorithm²⁰ used to optimize T_2 -selective pulses in this work, particularly those used in Figure 4 (PDF)

AUTHOR INFORMATION

Corresponding Author

*E-mail: jwalls@miami.edu. Phone: +001 305 2844570. Fax: +001 305 2844571.

ORCID ®

Jamie D. Walls: 0000-0003-4813-852X

Notes

The authors declare no competing financial interest.

ACKNOWLEDGMENTS

This material is based upon work supported by National Science Foundation Grants CHE-1626015 and CHE-1807724.

REFERENCES

- (1) Stejskal, E. O.; Tanner, J. E. Spin diffusion measurements: spin echoes in the presence of a time-dependent field gradient. *J. Chem. Phys.* **1965**, *42*, 288–292.
- (2) Morris, K. F.; Johnson, C. S. Diffusion-ordered two-dimensional nuclear magnetic resonance spectroscopy. *J. Am. Chem. Soc.* **1992**, 114, 3139–3141.
- (3) Barjat, H.; Morris, G. A.; Smart, S.; Swanson, A. G.; Williams, S. C. R. High-Resolution Diffusion-Ordered 2D Spectroscopy (HR-DOSY)- A New Toool for the Analysis of Complex Mixtures. *J. Magn. Reson., Ser. B* **1995**, *108*, 170–172.
- (4) Hajduk, P. J.; Olejniczak, E. T.; Fesik, S. W. One-dimensional Relaxation- and Diffusion-edited NMR Methods for Screening Compounds That Bind to Macromolecules. *J. Am. Chem. Soc.* **1997**, 119, 12257–12261.
- (5) Chen, A.; Johnson, C. S.; Lin, M.; Shapiro, M. J. Chemical Exchange in Diffusion NMR Experiments. *J. Am. Chem. Soc.* **1998**, 120, 9094–9095.
- (6) Callaghan, P. T.; Furó, I. Diffusion-diffusion correlation and exchange as a signature for local order and dynamics. *J. Chem. Phys.* **2004**, *120*, 4032–4038.
- (7) van Zijl, P. C. M.; Moonen, C. T.W Complete water suppression for solutions of large molecules based on diffusional differences between solute and solvent (DRYCLEAN). *J. Magn. Reson.* **1990**, *87*, 18–25.
- (8) Stoller, S. D.; Happer, W.; Dyson, F. J. Transverse spin relaxation in inhomogeneous magnetic fields. *Phys. Rev. A: At., Mol., Opt. Phys.* **1991**, *44*, 7459–7477.
- (9) de Swiet, T. M.; Sen, P. N. Decay of nuclear magnetization by bounded diffusion in a constant field gradient. *J. Chem. Phys.* **1994**, 100, 5597–5604.
- (10) Havel, T. F.; Sharf, Y.; Viola, L.; Cory, D. G. Hadamard products of product operators and the design of gradient-diffusion experiments for simulating decoherence by NMR spectroscopy. *Phys. Lett. A* **2001**, *280*, 282–288.
- (11) Rourke, D. E.; Bush, S. D. Inversion of the bloch equations with T-2 relaxation: An application of the dressing method. *Phys. Rev. E: Stat. Phys., Plasmas, Fluids, Relat. Interdiscip. Top.* **1998**, *57*, 7216–7230.
- (12) Bush, S. D.; Rourke, D. E.; Kaiser, L. G.; Pines, A. Relaxation selective magnetic resonance imaging. *Chem. Phys. Lett.* **1999**, 311, 379–384.
- (13) Lapert, M.; Zhang, Y.; Janich, M. A.; Glaser, S. J.; Sugny, D. Exploring the physical limits of saturation contrast in Magnetic resonance imaging. *Sci. Rep.* **2012**, *2*, 589.
- (14) Lopez, C. J.; Lu, W.; Walls, J. D. Relaxation Selective Pulses in Fast Relaxing Systems. J. Magn. Reson. 2014, 242, 95–106.
- (15) Jeener, J. Superoperators in magnetic resonance. Adv. Magn. Opt. Reson. 1982, 10, 1-51.
- (16) Sinnaeve, D. The Stejskal-Tanner Equation Generalized for Any Gradient Shape- An Overview of Most Pulse Sequences Measuring Free Diffusion. *Concepts Magn. Reson., Part A* **2012**, 40A, 39–65.
- (17) Levitt, M. H.; Dibari, L. Steady-State in Magnetic Resonance Pulse Experiments. *Phys. Rev. Lett.* **1992**, *69*, 3124–3127.
- (18) Walls, J. D.; Coomes, A. Pseudorandom Selective Excitation in NMR. J. Magn. Reson. 2011, 212, 186–196.

- (19) Garwood, M.; DelaBarre, L. The return of the frequency sweep: designing adiabatic pulses for contemporary NMR. *J. Magn. Reson.* **2001**, *153*, 155–177.
- (20) Khaneja, N.; Reiss, T.; Kehlet, C.; Schulte-Herbruggen, T.; Glaser, S. J. Optimal Control of Coupled Spin Dynamics: Design of NMR Pulse Sequences by Gradient Ascent Algorithms. *J. Magn. Reson.* **2005**, *172*, 296–305.
- (21) Topgaard, D. Multidimensional diffusion MRI. J. Magn. Reson. 2017, 275, 98–113.
- (22) Patt, S. L.; Sykes, B. D. Water Elminated Fourier-Transform NMR-Spectroscopy. *J. Chem. Phys.* **1972**, *56*, 3182–3184.
- (23) Carr, H. Y.; Purcell, E. M. Effects of diffusion on free precession in nuclear magnetic resonance experiments. *Phys. Rev.* **1954**, *94*, 630–638
- (24) Meiboom, S.; Gill, D. Modified Spin-echo method for measuring nuclear relaxation times. *Rev. Sci. Instrum.* **1958**, 29, 688–691.
- (25) Frahm, J.; Haase, A.; Matthaei, D. Rapid NMR Imaging of Dynamic Processes Using the FLASH Technique. *Magn. Reson. Med.* **1986**, *3*, 321–327.

Supporting Information for "Diffusion Selective Pulses"

Zhaoyuan Gong and Jamie D. Walls*

Department of Chemistry, University of Miami, Coral Gables, FL 33146

E-mail: jwalls@miami.edu

Phone: +001 305 284-4570. Fax: +001 305 284-4571

The following supporting information is provided: first, a few details about the calculations and superoperators introduced in the manuscript are provided. This is followed by a more in depth discussion about the mechanism behind the relaxation selective pulses used in this work. Plots of the diffusion selective pulses used in this work are also given, along with a table of spectral integrals in the 1:1:1:3 H₂O/DMSO/acetone/D₂O solution after application of diffusion selective pulses. Finally, details about the optimization algorithms used in generating relaxation/diffusion selective pulses are provided.

Additional details about theory in main paper

In Eq. (2) of the main paper, $\widehat{H}_{RF}(\omega_{RF}(t), \phi(t))$, which is the superoperator representing an RF pulse of amplitude $\omega_{RF}(t)$ and phase $\phi(t)$, is given by:

$$\widehat{H}_{RF}(\omega_{RF}, \phi) = i\omega_{RF} \begin{pmatrix} 0 & 0 & 0 & 0 \\ 0 & 0 & \frac{e^{-i\phi}}{2} & -\frac{e^{i\phi}}{2} \\ 0 & e^{i\phi} & 0 & 0 \\ 0 & -e^{-i\phi} & 0 & 0 \end{pmatrix}$$
(1)

The basic building block of implementing a diffusion selective pulse consists of placing an RF pulse in the middle of a GRE block, as shown in Fig. 2(A) in the main text. The reason for this is that the "zeroth"-order average Liouvillian for the k^{th} block for k=1 to $k=N_c$, $\overline{\mathcal{L}^k}_{GRE}$ in Eq. (7) of the main text, is correct to second-order in terms of average Liouvillian theory due to the symmetry of the evolution. Furthermore, keeping only the zeroth-order average Liouvillian in Eq. (7) of the main text and neglecting second-order and higher contributions is a reasonable approximation as long as $\theta_k = 2\pi\nu_{RF}t_k \ll \frac{\pi}{3}$. Furthermore, the condition $|\omega_I\tau_c| \ll \frac{\pi}{3}$ should also be observed in order to avoid any DANTE-like resonances due to the inherent periodicity of the implementation of diffusion selective pulse given in Fig. 2(A) of the main text. In principle,

breaking this periodicity could be accomplished by varying the delays between GRE blocks, for example, although one would need to be careful that the same effective $T_2^{\rm Eff.}$ was being generated in the different GRE blocks.

Mechanism behind relaxation selective pulses

As described in the main text, the majority of relaxation selective pulses consist of two basic steps: first, the initial equilibrium magnetization is attenuated and inverted by the relaxation selection pulse over a time $T_p - \tau_D$ from \vec{M}_{eq} to $\vec{M}^{DSP}(T_2, T_1, T_p - \tau_D)$, which points along the $-\hat{z}$ -direction. The attenuation under the diffusion selective pulse, $\left| \vec{M}^{DSP}(T_2, T_1, T_p - \tau_D) \right|$, depends upon the T_1 and T_2 of spins and the details of the relaxation selective pulse. In the second step, the inverted magnetization undergoes a partial inversion recovery (T_1 relaxation) for a time $\tau_D = T_1^{\rm Sel} \ln \left(\frac{M^{DSP}(T_2^{\rm Sel}, T_1^{\rm Sel})}{M_{eq}} + 1 \right)$, giving a total pulse length of T_p for the relaxation selective pulse. At the end of the relaxation selective pulse, those spins with $T_2 = T_2^{\rm Sel}$ and $T_1 = T_1^{\rm Sel}$ have had their magnetization nulled, i.e., $\left| M^{DSP}(T_2^{\rm Sel}, T_1^{\rm Sel}, T_p) \right| \approx 0$. Typically for spins with $T_2 < T_2^{\rm Sel}$, $\left| \vec{M}^{DSP}(T_2, T_1, T_p - \tau_D) \right| < \left| \vec{M}^{DSP}(T_2^{\rm Sel}, T_1^{\rm Sel}, T_p - \tau_D) \right|$ and thus $\vec{M}^{DSP}(T_2, T_1, T_p)$ ends up with \hat{z} -magnetization oriented along the $+\hat{z}$ -direction after the inversion recovery period. For species with $T_2 > T_2^{\rm Sel}$,

 $\left| \vec{M}^{DSP}(T_2, T_1, T_p - au_D)
ight| > \left| \vec{M}^{DSP}(T_2^{\rm Sel}, T_1^{\rm Sel}, T_p - au_D)
ight|$ and thus $\vec{M}^{DSP}(T_2, T_1, T_p)$ ends up with \hat{z} -magnetization still oriented along the $-\hat{z}$ -direction after the inversion recovery period. This behavior is illustrated in Fig. 1 which shows the trajectories for magnetization under diffusion selective pulses used in Fig. 2 and Fig. 4(C) of the main paper (the latter pulse is given in Fig. 3(A) in Supporting Information). As discussed above, the magnetization is inverted in all cases and then undergoes T_1 relaxation whereby those species with $T_2 = T_2^{\rm Sel}$ are suppressed.

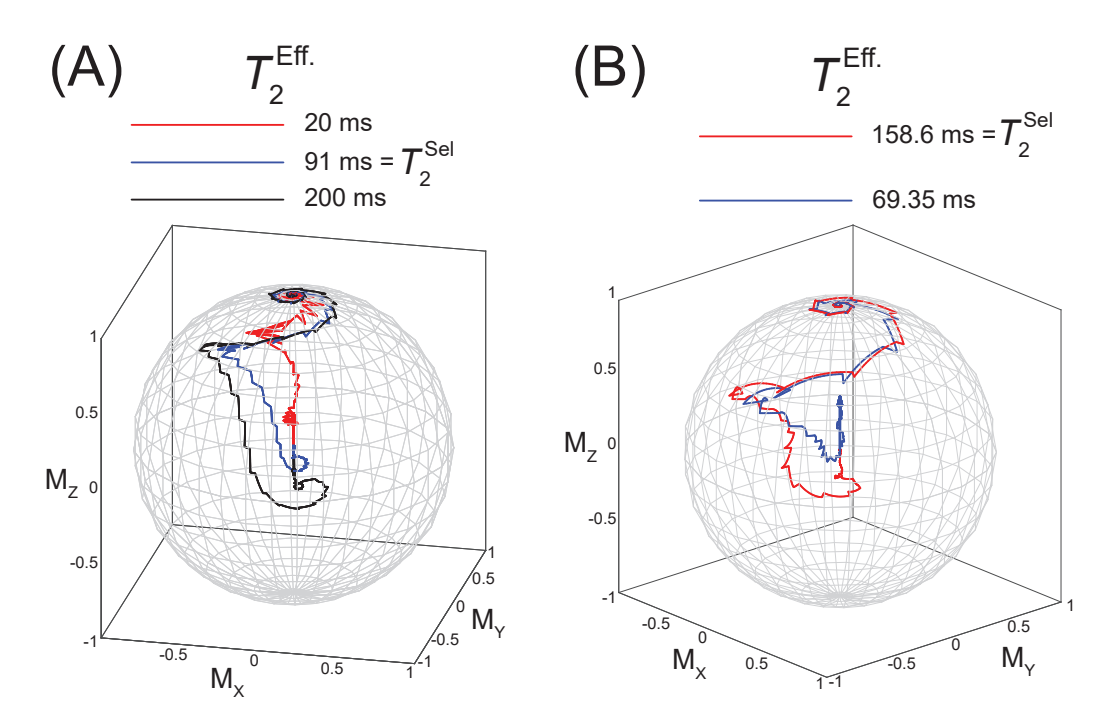


Figure 1: Trajectories of the magnetization vectors with different values of T_2 under two different diffusion selective pulses. (A) Under the diffusion selective pulse designed to suppress the magnetization for species with $T_2^{\rm Sel}=91~{\rm ms}~(T_p=1.8408~{\rm s})$ used in Fig. 2 in the main manuscript, the trajectories of the magnetization for species with $T_2=20~{\rm ms}~({\rm red~curve}), T_2=91~{\rm ms}=T_2^{\rm Sel}$ (blue curve), and $T_2=200~{\rm ms}~({\rm black~curve})$ are shown. In all case, the magnetization is inverted from equilibrium, after which the magnetization undergoes inversion recovery. For $T_2=20~{\rm ms}< T_2^{\rm Sel}$ (red curve), the magnetization ends up being oriented along the $+\hat{z}$ -direction; for $T_2=200~{\rm ms}>T_2^{\rm Sel}$ (black curve), the magnetization ends up being along $-\hat{z}$ -direction, and for $T_2=T_2^{\rm Sel}=91~{\rm ms}$ (blue curve), the magnetization ends up being nulled at time $T_p=1.8408~{\rm s}$. (B) The trajectories of the magnetization during the diffusion selective pulse used in Fig. 4(C) in the main paper [and given in Fig. 3(A)] are shown for species with $T_2=69.35~{\rm ms}$ (blue curve) and $T_2=T_2^{\rm Sel}=158.6~{\rm ms}$ (red curve). Similar to the trajectories in (A), the diffusion selective pulse ends up inverting the magnetization of both species although the species with $T_2=69.35~{\rm ms}< T_2^{\rm Sel}$ ends up with magnetization along the $+\hat{z}$ -direction (blue curve) whereas the species with $T_2=T_2^{\rm Sel}=158.6~{\rm ms}$ ends up being nulled at the end of the diffusion selective pulse.

Diffusion selective pulses used in Figs. 3 and 4 of the main text

Figures 2 and 3 give the pulse lengths, t_k , and phases ϕ_k , for the diffusion selective pulses used in Fig. 3 and Fig. 4 in the main text. In Fig. 2, the diffusion selective pulses were implemented using the sequence in Fig. 2(A) in order to selectively suppress signals in a 1:1:1:3 v/v/v/v H₂O/DMSO/acetone/D₂O solution based upon the effective relaxation times under the GRE blocks. The water, acetone, and DMSO resonances were suppressed using the diffusion selective pulses given in Fig. 2(B), 2(C), and 2(D), respectively.

The integrals of the spectra in the $H_2O/DMSO/acetone$ solution [Fig. 3(C) in the main text] from the remaining transverse and $\hat{z}-$ magnetization after application of diffusion selective pulses given in Fig. 2 are given in Table 1. In most cases, the resulting attenuation of magnetization after application of the diffusion selective pulses was typically less than the theoretical predictions given by Eq. (6) in the main text, although in some cases larger signals were observed as given in Table 1. In these cases, differences in $T_{1,I}$ and/or chemical shifts can reduce the overall magnetization attenuation of the diffusion selective pulses as predicted from Eq. (6) in the main text. In Fig. 3, diffusion selective pulses that were used in the imaging experiments shown in Figure 4 of the main text are present with additional details given in Fig. 3's caption.

Application of the GRAPE method to optimize RF pulses

In many problems in NMR, we are interested in finding an RF pulse, $\left(\omega^{RF}(t)\right)_{\phi(t)}$, that minimizes a given cost functional, $\Phi\left[\Omega_{\text{spectral}}, (\omega^{RF}(t))_{\phi(t)}, \eta_{RF}, \omega_{Z}, \vec{M}(T_p)\right]$, which depends upon the spectral parameters $\left[\Omega_{\text{spectral}} \in T_1, T_2, \text{ chemical shifts, J-couplings, etc.}\right]$, RF and B_0 inhomogeneity, which are represented by η_{RF} and ω_{Z} , respectively [where the dimensionless parameter η_{RF} represents an RF scaling factor with $\eta_{RF}=1$ for a perfectly calibrated pulse, and ω_{Z} represents a local resonance offset], and the final state of the magnetization at the end of the RF pulse of length T_p ,

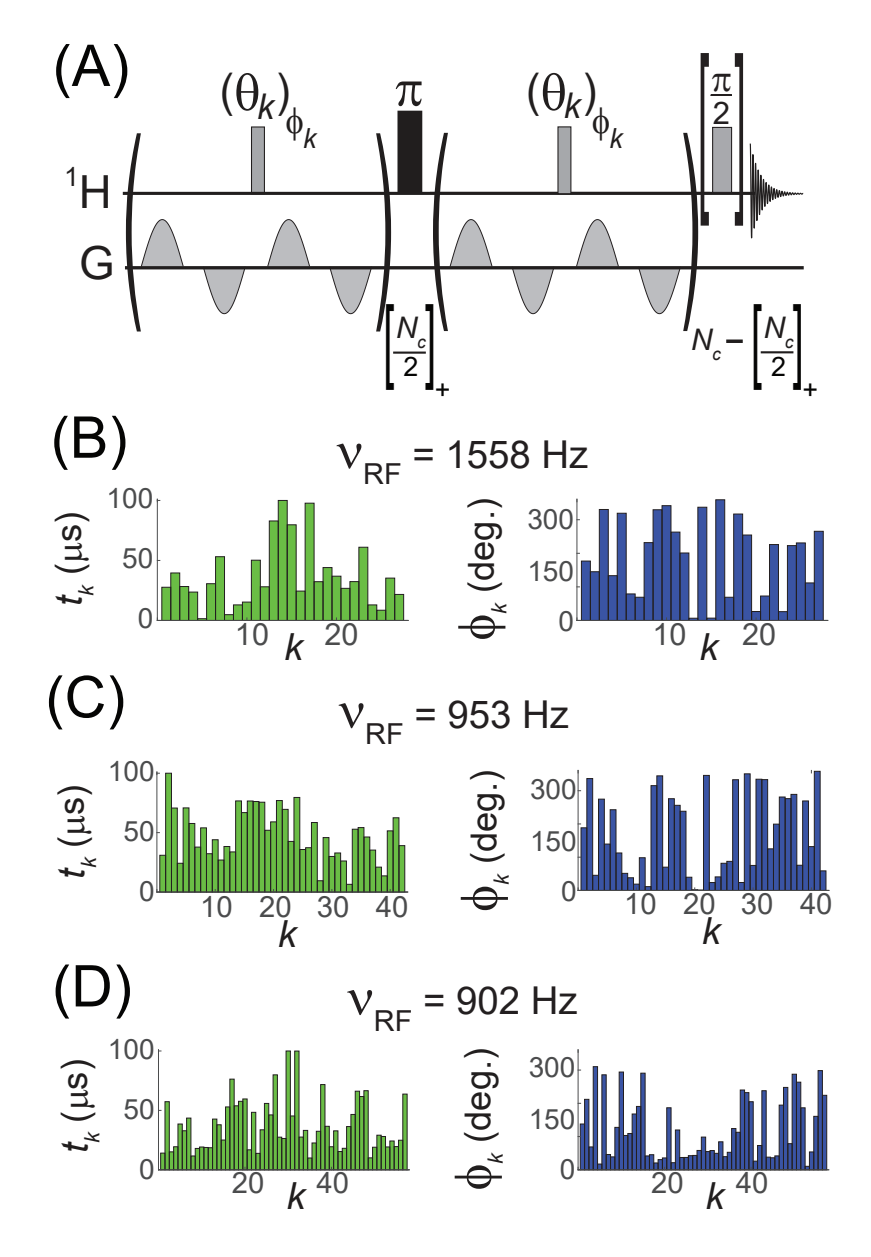


Figure 2: Diffusion selective pulses designed to selectively suppress signals in a 1:1:1:3 H₂O/DMSO/acetone/D₂O solution used in Fig. 3 of the main text. (A) The basic pulse sequence used to implement the diffusion selective pulses, where a π -pulse was placed roughly in the middle ([z]₊ = ceiling of z) of the sequence. In all experiments, g=44.7 G/cm, $\delta=3$ ms, $\Delta=4$ ms, $t_d=400~\mu\text{s},~\tau_c=15.6$ ms, and the RF transmitter was placed at the average frequency offset of $\delta_{\text{transmitter}}=3.22$ ppm. (B) Diffusion selective pulse ($N_c=27,~\nu_{RF}=1558$ Hz, $T_p=421.2$ ms, and $T_2^{\text{Sel}}=37$ ms) designed to suppress the water resonance. (C) Diffusion selective pulse ($N_c=42,~\nu_{RF}=953$ Hz, $T_p=655.2$ ms, and $T_2^{\text{Sel}}=58$ ms) designed to suppress the acetone resonance. (D) Diffusion selective pulse ($N_c=57,~\nu_{RF}=902$ Hz, $T_p=889.2$ ms, and $T_2^{\text{Sel}}=71$ ms) designed to suppress the DMSO resonance. The spectra after application of the diffusion selective pulses were given in Fig. 3(C) of the main text with the corresponding integrals of the spectra given in Table 1.

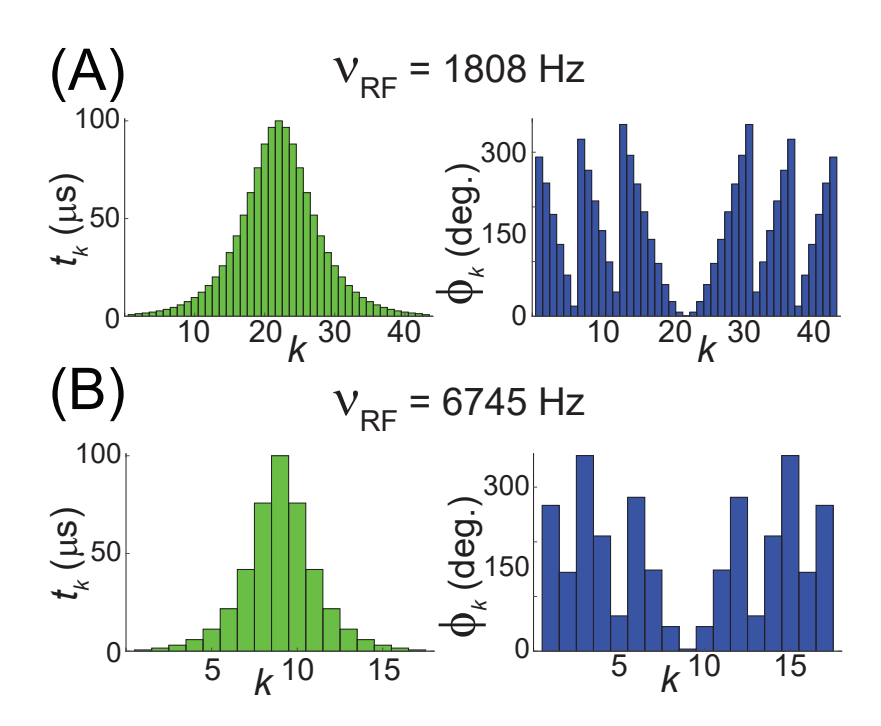


Figure 3: Diffusion selective pulses designed to selectively suppress signals in an imaging phantom used in Figure 4 of the main text. In all experiments, g=23.92 G/cm, $\delta=3$ ms, $\Delta=5.11$ ms, $t_d=500\,\mu\text{s}$, and $\tau_c=18.45$ ms. (B) Diffusion selective pulse ($N_c=43$, $\nu_{RF}=1808$ Hz, $T_p=793.35$ ms, and $T_2^{\text{Sel}}=158.6$ ms) designed to suppress the water resonance in a 1:1 v/v H₂O/DMSO-d₆ solution with pH= 4.56 (placed in 2mm coaxial insert). (C) Diffusion selective pulse ($N_c=17$, $\nu_{RF}=6745$ Hz, $T_p=313.65$ ms, and $T_2^{\text{Sel}}=69.35$ ms) designed to suppress the water resonance in a [Gd⁺³]=88 μ M solution in 1:1 v/v H₂O/D₂O sample (placed in outer 5mm tube). Images taken after application of these diffusion selective pulses were given in Fig. 4(C) and 4(D) of the main text.

Table 1: Observed integrals for diffusion-selective pulses [Fig. 2] applied to a 1:1:1:3 v/v/v/v DMSO/acetone/H₂O/D₂O solution [Fig. 3 from main text]

 $\vec{M}(T_p) = M_Z(T_p)\hat{z} + M_X(T_p)\hat{x} + M_Y(T_p)\hat{y}$, which can be calculated from:

$$\mathbf{M}(T_{p}) = \begin{pmatrix} 1 \\ M_{Z}(T_{p}) \\ M_{X}(T_{p}) \\ M_{Y}(T_{p}) \end{pmatrix} = 1 + \vec{M}(T_{p})$$

$$= \widehat{T} \exp\left(\int_{0}^{T_{p}} dt' \left[\eta_{RF} \left(\omega_{X}^{RF}(t') \hat{I}_{X} + \omega_{Y}^{RF}(t') \hat{I}_{Y} \right) + \omega_{Z} \hat{I}_{Z} + \hat{\mathcal{L}}(\Omega_{\text{spectral}}) \right] \right) \mathbf{M}(0) \qquad (2)$$

$$\vec{M}(T_{p}) = \left(\widehat{z} (\widehat{z})^{\text{T}} + \widehat{x} (\widehat{x})^{\text{T}} + \widehat{y} (\widehat{y})^{\text{T}} \right) \widehat{\mathbf{M}}(T_{p}) \qquad (3)$$

where
$$\widehat{T}$$
 represents the Dyson-time ordering operator, $\widehat{z} = \begin{pmatrix} 0 \\ 1 \\ 0 \\ 0 \end{pmatrix}$, $\widehat{x} = \begin{pmatrix} 0 \\ 0 \\ 1 \\ 0 \end{pmatrix}$, $\widehat{y} = \begin{pmatrix} 0 \\ 0 \\ 0 \\ 1 \end{pmatrix}$,

and $\mathbf{M}(0)=1+\vec{M}(0)=1+M_{eq}\widehat{z}$. In Eq. (2), $\widehat{\hat{I}}_X$, $\widehat{\hat{I}}_Y$ and $\widehat{\hat{I}}_Z$ represent spin-1/2 superoperators,

which are given by:

$$\widehat{\hat{I}}_{Z} = \begin{pmatrix}
0 & 0 & 0 & 0 \\
0 & 0 & 0 & 0 \\
0 & 0 & 0 & 1 \\
0 & 0 & -1 & 0
\end{pmatrix}$$

$$\widehat{\hat{I}}_{X} = \begin{pmatrix}
0 & 0 & 0 & 0 \\
0 & 0 & 0 & -1 \\
0 & 0 & 0 & 0 \\
0 & 1 & 0 & 0
\end{pmatrix}$$

$$\widehat{\hat{I}}_{Y} = \begin{pmatrix}
0 & 0 & 0 & 0 \\
0 & 0 & 1 & 0 \\
0 & -1 & 0 & 0 \\
0 & 0 & 0 & 0
\end{pmatrix}$$
(4)

and $\widehat{\mathcal{L}}(\Omega_{\text{spectral}})$ represents the time-independent Liouvillian during the time T_p . When $\left(\omega^{RF}(t)\right)_{\phi(t)}$ can be approximated by a series of N, piecewise constant rectangular pulses as illustrated in Fig. 4, where the amplitude, phase, and length of the $k^{th}-$ pulse is given by ω_k^{RF} , ϕ_k , and τ_k , respectively, then $\mathbf{M}(T_p)$ with $T_p = \sum_{k=1}^N \tau_k$ can be approximated by:

$$\mathbf{M}(T_p) \approx \left(\widehat{T} \prod_{k=1}^{N} \widehat{V}_k(\Omega_{\text{spectral}}, \omega_Z, \eta_{RF}, \omega_{X,k}^{RF}, \omega_{Y,k}^{RF}, \tau_k)\right) \mathbf{M}(0)$$

$$\approx 1 + \vec{M}(T_p) = 1 + \left(\widehat{z}(\widehat{z})^{\mathsf{T}} + \widehat{x}(\widehat{x})^{\mathsf{T}} + \widehat{y}(\widehat{y})^{\mathsf{T}}\right) \widehat{\mathbf{M}}(T_p)$$
(5)

where $\omega_{X,k}^{RF} = \omega_k^{RF}\cos(\phi_k)$, $\omega_{Y,k}^{RF} = \omega_k^{RF}\sin(\phi_k)$, and

$$\widehat{V}_{k}(\Omega_{\text{spectral}}, \omega_{Z}, \eta_{RF}, \omega_{X,k}^{RF}, \omega_{Y,k}^{RF}, \tau_{k}) = \exp\left(\tau_{k} \left[\eta_{RF} \left(\omega_{X,k}^{RF} \widehat{\widehat{I}}_{X} + \omega_{Y,k}^{RF} \widehat{\widehat{I}}_{Y} \right) + \omega_{Z} \widehat{\widehat{I}}_{Z} + \widehat{\widehat{\mathcal{L}}}(\Omega_{\text{spectral}}) \right] \right)$$

$$(6)$$

represents the propagator during the time $\sum_{j=1}^{k-1} \tau_j \le t \le \sum_{j=1}^k \tau_j$ under the k^{th} rectangular pulse.

For a T_2- selective pulse, the cost functional $\Phi\left[\Omega_{\mathrm{spectral}},\eta_{RF},\omega_Z,\vec{M}(T_p)\right]$ should be minimized for a $\left(\omega^{RF}(t)\right)_{\phi(t)}$ that results in $\left|\vec{M}(T_p)\right|\approx 0$ for $T_2=T_2^{\mathrm{Sel}}$ while minimally attenuating $|\vec{M}(T_p)|$ for those spins with $T_2\neq T_2^{\mathrm{Sel}}$. One way to find such an $\left(\omega^{RF}(t)\right)_{\phi(t)}$ is by using the GRAPE algorithm. The GRAPE algorithm works as follows: defining the following propagators for k=1 to k=N:

$$\widehat{\widehat{U}}_{k}^{F} = \widehat{T} \prod_{j=1}^{k} \widehat{\widehat{V}}_{j}(\Omega_{\text{spectral}}, \omega_{Z}, \eta_{RF}, \omega_{X,j}^{RF}, \omega_{Y,j}^{RF}, \tau_{j})$$

$$(7)$$

along with $\widehat{\widehat{U}}_{1}^{B}=\widehat{\widehat{1}},$ and

$$\widehat{\widehat{U}}_{k}^{B} = \widehat{T} \prod_{j=2}^{k} \widehat{\widehat{V}}_{N-j+2}(\Omega_{\text{spectral}}, \omega_{Z}, \eta_{RF}, \omega_{X,N-j+2}^{RF}, \omega_{Y,N-j+2}^{RF}, \tau_{N-j+2})$$
(8)

for k=2 to k=N, $\vec{M}(T_p)$ can be determined from Eq. (5) by:

$$\vec{M}(T_p) = \left(\widehat{z}(\widehat{z})^{\mathsf{T}} + \widehat{x}(\widehat{x})^{\mathsf{T}} + \widehat{y}(\widehat{y})^{\mathsf{T}}\right) \widehat{\hat{U}}_N^F \widehat{\mathbf{M}}(0)$$
(9)

where we used the fact that $\mathbf{M}(T_p) = \widehat{\widehat{U}}_N^F \mathbf{M}(0)$. Denoting $\vec{\omega}_X^{RF} = \left(\omega_{X,1}^{RF}, \, \omega_{X,2}^{RF}, \, \cdots, \, \omega_{X,N-1}^{RF}, \, \omega_{X,N}^{RF}\right)$ and $\vec{\omega}_Y^{RF} = \left(\omega_{Y,1}^{RF}, \, \omega_{Y,2}^{RF}, \, \cdots, \, \omega_{Y,N-1}^{RF}, \, \omega_{Y,N}^{RF}\right)$, the GRAPE algorithm finds the appropriate $\vec{\omega}_X^{RF}$ and $\vec{\omega}_Y^{RF}$ that minimize Φ by updating the k^{th} pulse to $\left(\omega_{X,k}^{RF}\right)^{\text{new}} = \left(\omega_{X,k}^{RF}\right)^{\text{old}} - \lambda_{\text{step}} \overline{\delta \omega}_{X,k}$ and $\left(\omega_{Y,k}^{RF}\right)^{\text{new}} = \left(\omega_{Y,k}^{RF}\right)^{\text{old}} - \lambda_{\text{step}} \overline{\delta \omega}_{Y,k}$ for k = 1 to k = N, where:

$$\overline{\delta\omega}_{X,k} = \left\langle \left(\frac{\delta\Phi}{\delta M_Z} \overline{z}^{\mathsf{T}} + \frac{\delta\Phi}{\delta M_X} \overline{x}^{\mathsf{T}} + \frac{\delta\Phi}{\delta M_Y} \overline{y}^{\mathsf{T}} \right) \left(\eta_{RF} \tau_k \widehat{\widehat{U}}_{N-k+1}^B \widehat{\widehat{H}}_X \widehat{\widehat{U}}_k^F \widehat{\mathbf{M}}(0) \right) \right\rangle \\
\overline{\delta\omega}_{Y,k} = \left\langle \left(\frac{\delta\Phi}{\delta M_Z} \overline{z}^{\mathsf{T}} + \frac{\delta\Phi}{\delta M_X} \overline{x}^{\mathsf{T}} + \frac{\delta\Phi}{\delta M_Y} \overline{y}^{\mathsf{T}} \right) \left(\eta_{RF} \tau_k \widehat{\widehat{U}}_{N-k+1}^B \widehat{\widehat{H}}_Y \widehat{\widehat{U}}_k^F \widehat{\mathbf{M}}(0) \right) \right\rangle \tag{10}$$

In Eq. (10), $\langle \cdots \rangle$ represents a (possible) average over parameters [e.g., T_2 's, η_{RF} , ω_Z , etc.], and

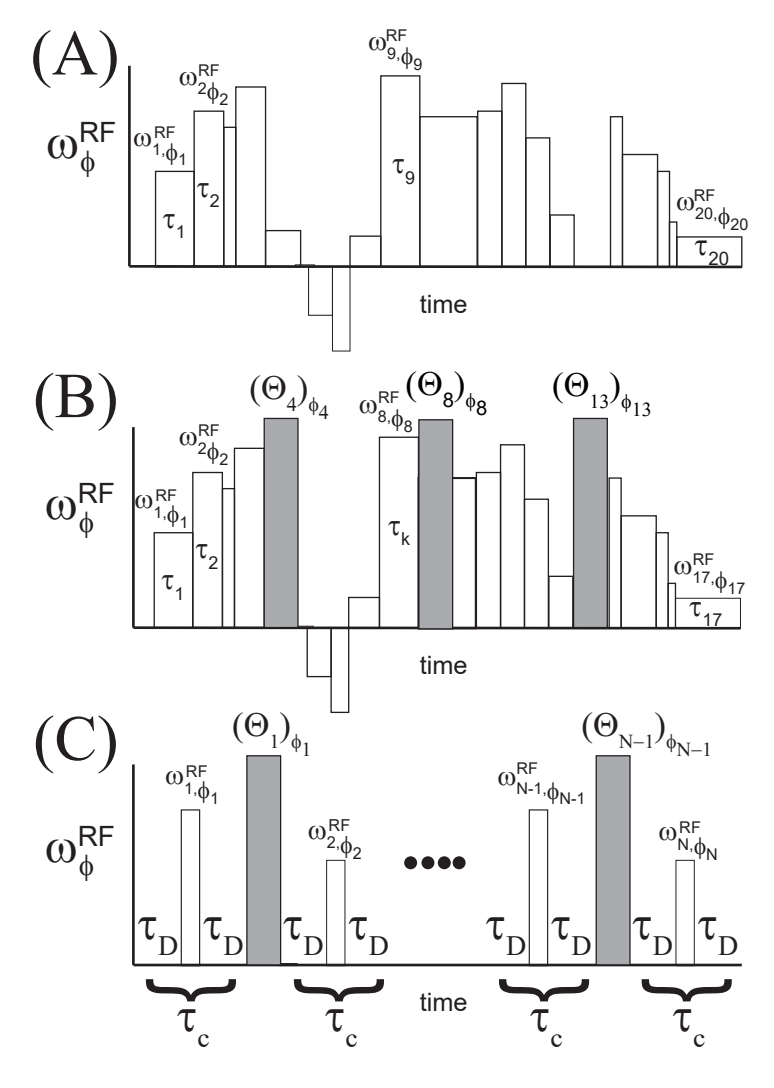


Figure 4: (A) An RF pulse, $\left(\omega^{RF}(t)\right)_{\phi(t)}$, that is approximated by N, piecewise constant rectangular pulses, where the k^{th} pulse has amplitude, phase, and length of ω_k^{RF} , ϕ_k , and τ_k , respectively. As illustrated in (A), the $\left(\omega^{RF}(t)\right)_{\phi(t)}$ was approximated by N=20 rectangular pulses. In the GRAPE algorithm, the individual ω_k^{RF} and ϕ_k are optimized by iterating Eq. (10). (B) The GRAPE algorithm can also be used to optimize the individual ω_k^{RF} and ϕ_k in the presence of fixed RF pulses $[(\Theta_4)_{\phi_4}-,(\Theta_8)_{\phi_8}-$, and $(\Theta_{13})_{\phi_{13}}-$ pulses as illustrated in (B)] by iterating Eq. (15). (C) For a pulse sequence consisting of N small-flip $(\theta_k)_{\phi_k}-$ pulses with $\theta_k=\omega_k^{RF}t_p$ applied in between periods of free evolution of time τ_D (with $\tau_c=2\tau_D+t_p$) and fixed RF pulses, the individual ω_k^{RF} and ϕ_k of the $(\theta_k)_{\phi_k}-$ pulses can be optimized by iterating Eq. (19).

 $\frac{\delta\Phi}{\delta M_j}$ represents functional derivatives of Φ with respect to M_j for j=X,Y,Z. In this case, the algorithm is iterated until convergence is achieved (additional details of the implementation, such as line searches to determine the best λ_{step} and time scaling, have been previously reported⁴).

Optimizing $\left(\omega^{RF}(t)\right)_{\phi(t)}$ in the presence of a fixed set of RF pulses

In some instances, $\left(\omega^{RF}(t)\right)_{\phi(t)}$ needs to be applied in the presence of a series of fixed, RF pulses, e.g., applying a selective excitation pulse in the presence of homonuclear decoupling or requiring a $\pi-$ pulse be applied in the middle of the sequence to refocus B_0 inhomogeneity, etc. In this case, a modified version of the GRAPE algorithm can be employed. Consider determining a $\left(\omega^{RF}(t)\right)_{\phi(t)}$ that minimizes some cost function Φ in the presence of a set of fixed RF pulses. Assume again that $\left(\omega^{RF}(t)\right)_{\phi(t)}$ can be represented by N, piecewise constant rectangular pulses, but with up to N additional, fixed RF pulses that are interspersed within the sequence. This is illustrated in Fig. 4(B), where N=17, and three different, fixed RF pulses are applied: a $(\Theta_4)_{\phi_4}-$ pulse [applied directly after the $\left(\omega^{RF}_8\right)_{\phi_8}-$ pulse [applied directly after the $\left(\omega^{RF}_8\right)_{\phi_8}-$ pulse], and a $\left(\Theta_{13}\right)_{\phi_{13}}-$ pulse [applied directly after the $\left(\omega^{RF}_{13}\right)_{\phi_{13}}-$ pulse]. Defining the following propagators for k=1 to k=N:

$$\widehat{\widehat{U}}_{RF,k}^{F} = \widehat{T} \prod_{j=1}^{k} \widehat{\widehat{R}}_{j} \widehat{\widehat{V}}_{j} (\Omega_{\text{spectral}}, \omega_{Z}, \eta_{RF}, \omega_{X,j}^{RF}, \omega_{Y,j}^{RF}, \tau_{j})$$
(11)

where $\widehat{\widehat{V}}_{j}$ is given in Eq. (6), and

$$\widehat{\widehat{R}}_{j} = \exp\left(t_{j} \left[\eta_{RF} \left(\frac{\Theta_{j}}{t_{j}} \cos(\phi_{j}) \widehat{\widehat{I}}_{X} + \frac{\Theta_{j}}{t_{j}} \sin(\phi_{j}) \widehat{\widehat{I}}_{Y} \right) + \omega_{Z} \widehat{\widehat{I}}_{Z} + \widehat{\widehat{\mathcal{L}}}(\Omega'_{\text{Spectral}}) \right] \right)$$
(12)

represents the propagator for a rectangular RF pulse pulse of length t_j with a nominal flip angle of $\Theta_j \neq 0$. If $\Theta_j = 0$, then $t_j = 0$ and so $\widehat{R}_j = \widehat{1}$ representing the fact that no RF pulse was applied.

Note that in Eq. (12), $\widehat{\widehat{\mathcal{L}}}(\Omega'_{\text{Spectral}})$ need not be the same as $\widehat{\widehat{\mathcal{L}}}(\Omega_{\text{spectral}})$ found in Eq. (6). Further define $\widehat{\widehat{U}}_{RF,1}^B = \widehat{\widehat{1}}$, and

$$\widehat{\widehat{U}}_{k}^{B} = \widehat{T} \prod_{j=2}^{k} \widehat{\widehat{R}}_{N-j+2} \widehat{\widehat{V}}_{N-j+2} (\Omega_{\text{spectral}}, \omega_{Z}, \eta_{RF}, \omega_{X,N-j+2}^{RF}, \omega_{Y,N-j+2}^{RF}, \tau_{N-j+2})$$

$$(13)$$

for k=2 to k=N, $\vec{M}(T_p)$ can be written as:

$$\vec{M}(T_p) = \left(\widehat{z}(\widehat{z})^{\mathsf{T}} + \widehat{x}(\widehat{x})^{\mathsf{T}} + \widehat{y}(\widehat{y})^{\mathsf{T}}\right) \widehat{\widehat{U}}_{RF,N}^F \widehat{\mathbf{M}}(0)$$
(14)

In this case, the GRAPE algorithm can be used to find the appropriate $\vec{\omega}_X^{RF}$ and $\vec{\omega}_Y^{RF}$ that minimize Φ by updating the k^{th} pulse to $\left(\omega_{X,k}^{RF}\right)^{\mathrm{new}} = \left(\omega_{X,k}^{RF}\right)^{\mathrm{old}} - \lambda_{\mathrm{step}}\overline{\delta\omega}_{X,k}$ and $\left(\omega_{Y,k}^{RF}\right)^{\mathrm{new}} = \left(\omega_{Y,k}^{RF}\right)^{\mathrm{old}} - \lambda_{\mathrm{step}}\overline{\delta\omega}_{Y,k}$ for k=1 to k=N, where

$$\overline{\delta\omega}_{X,k} = \left\langle \left(\frac{\delta\Phi}{\delta M_Z} \overline{z}^{\mathsf{T}} + \frac{\delta\Phi}{\delta M_X} \overline{x}^{\mathsf{T}} + \frac{\delta\Phi}{\delta M_Y} \overline{y}^{\mathsf{T}} \right) \left(\eta_{RF} \tau_k \widehat{\widehat{U}}_{RF,N-k+1}^B \widehat{\widehat{R}}_k \widehat{\widehat{H}}_X \left(\widehat{\widehat{R}}_k \right)^{-1} \widehat{\widehat{U}}_{RF,k}^F \widehat{\mathbf{M}}(0) \right) \right\rangle
\overline{\delta\omega}_{Y,k} = \left\langle \left(\frac{\delta\Phi}{\delta M_Z} \overline{z}^{\mathsf{T}} + \frac{\delta\Phi}{\delta M_X} \overline{x}^{\mathsf{T}} + \frac{\delta\Phi}{\delta M_Y} \overline{y}^{\mathsf{T}} \right) \left(\eta_{RF} \tau_k \widehat{\widehat{U}}_{RF,N-k+1}^B \widehat{\widehat{R}}_k \widehat{\widehat{H}}_Y \left(\widehat{\widehat{R}}_k \right)^{-1} \widehat{\widehat{U}}_{RF,k}^F \widehat{\mathbf{M}}(0) \right) \right\rangle
(15)$$

Eq. (15) can be iterated until a desired level of convergence has been achieved.

Optimizing a series of small flip-angle pulses

When implementing diffusion selective pulses, pulsed field gradient blocks were utilized to generate an effective Liouvillian over the time τ_c , with $(\theta_k)_{\phi_k}$ – pulses of fixed length t_p placed in the middle of the pulsed field gradient blocks in order to generate a diffusion selective pulse, where $\theta_k = \omega_k^{RF} t_p$. This is illustrated in Fig. 4(C). In this case, for a given $\widehat{L}(\Omega''_{\text{spectral}})$ that was generated during the times τ_C , the various small-flip pulses can be optimized in order to minimize a given Φ .

Let $\widehat{\widehat{U}}_D = \exp\left(\tau_D \widehat{\widehat{L}}(\Omega''_{\text{spectral}})\right)$, and define the following propagators for k=1 to k=N:

$$\widehat{\widehat{U}}_{\text{delay},k}^{F} = \widehat{T} \prod_{j=1}^{k} \widehat{\widehat{R}}_{j} \widehat{\widehat{U}}_{D} \widehat{\widehat{V}}_{j} (\Omega_{\text{spectral}}, \omega_{Z}, \eta_{RF}, \omega_{X,j}^{RF}, \omega_{Y,j}^{RF}, t_{p}) \widehat{\widehat{U}}_{D}$$
(16)

where $\widehat{\widehat{V}}_j$ is given in Eq. (6), and $\widehat{\widehat{R}}_j$ is defined in Eq. (12). Note that $\widehat{\widehat{L}}(\Omega_{\text{spectral}})$ during the small-flip angle pulses may be different than the $\widehat{\widehat{L}}(\Omega''_{\text{spectral}})$ during the times τ_D and $\widehat{\widehat{L}}(\Omega'_{\text{spectral}})$ during the fixed RF pulses. Further, define $\widehat{\widehat{U}}_{\text{delay},1}^B = \widehat{\widehat{1}}$, and

$$\widehat{\widehat{U}}_{\text{delay},k}^{B} = \widehat{T} \prod_{j=2}^{k} \widehat{\widehat{R}}_{N-j+2} \widehat{\widehat{U}}_{D} \widehat{\widehat{V}}_{N-j+2} (\Omega_{\text{spectral}}, \omega_{Z}, \eta_{RF}, \omega_{X,N-j+2}^{RF}, \omega_{Y,N-j+2}^{RF}, t_{p}) \widehat{\widehat{U}}_{D}$$
(17)

for k=2 to k=N, then $\vec{M}(T_p)$ can be written as:

$$\vec{M}(T_p) = \left(\widehat{z}(\widehat{z})^{\mathsf{T}} + \widehat{x}(\widehat{x})^{\mathsf{T}} + \widehat{y}(\widehat{y})^{\mathsf{T}}\right) \widehat{\hat{U}}_{\mathrm{delay},N}^{F} \widehat{\mathbf{M}}(0)$$
(18)

In this case, the GRAPE algorithm finds the appropriate $\vec{\omega}_X^{RF}$ and $\vec{\omega}_Y^{RF}$ for the small-flip angle pulses that minimize Φ by updating the k^{th} pulse to $\left(\omega_{X,k}^{RF}\right)^{\text{new}} = \left(\omega_{X,k}^{RF}\right)^{\text{old}} - \lambda_{\text{step}}\overline{\delta\omega}_{X,k}$ and $\left(\omega_{Y,k}^{RF}\right)^{\text{new}} = \left(\omega_{Y,k}^{RF}\right)^{\text{old}} - \lambda_{\text{step}}\overline{\delta\omega}_{Y,k}$ for k=1 to k=N, where

$$\overline{\delta\omega}_{X,k} = \left\langle \left(\frac{\delta\Phi}{\delta M_Z} \overline{z}^{\mathrm{T}} + \frac{\delta\Phi}{\delta M_X} \overline{x}^{\mathrm{T}} + \frac{\delta\Phi}{\delta M_Y} \overline{y}^{\mathrm{T}} \right) \left(\eta_{RF} t_p \widehat{\widehat{U}}_{\mathrm{delay},N-k+1}^B \widehat{\widehat{R}}_k \widehat{\widehat{U}}_D \widehat{\widehat{H}}_X \left(\widehat{\widehat{U}}_D \right)^{-1} \left(\widehat{\widehat{R}}_k \right)^{-1} \widehat{\widehat{U}}_{\mathrm{delay},k}^F \widehat{\mathbf{M}}(0) \right) \right\rangle \\
\overline{\delta\omega}_{Y,k} = \left\langle \left(\frac{\delta\Phi}{\delta M_Z} \overline{z}^{\mathrm{T}} + \frac{\delta\Phi}{\delta M_X} \overline{x}^{\mathrm{T}} + \frac{\delta\Phi}{\delta M_Y} \overline{y}^{\mathrm{T}} \right) \left(\eta_{RF} t_p \widehat{\widehat{U}}_{\mathrm{delay},N-k+1}^B \widehat{\widehat{R}}_k \widehat{\widehat{U}}_D \widehat{\widehat{H}}_Y \left(\widehat{\widehat{U}}_D \right)^{-1} \left(\widehat{\widehat{R}}_k \right)^{-1} \widehat{\widehat{U}}_{\mathrm{delay},k}^F \widehat{\mathbf{M}}(0) \right) \right\rangle \tag{19}$$

Eq. (19) can be iterated until some desired level of convergence has been achieved. The diffusion selective pulses in Fig. 4 of the manuscript utilized this version of the GRAPE algorithm.

Acknowledgments

We would like to acknowledge support from the National Science Foundation under CHE - 1626015 and CHE - 1807724.

References

- (1) Levitt, M. H.; Dibari, L. Steady-State in Magnetic Resonance Pulse Experiments. *Phys. Rev. Lett.* **1992**, *69*, 3124–3127.
- (2) Walls, J. D.; Coomes, A. Pseudorandom Selective Excitation in NMR. *J. Mag. Res.* **2011**, *212*, 186–196.
- (3) Khaneja, N.; Reiss, T.; Kehlet, C.; Schulte-Herbruggen, T.; Glaser, S. J. Optimal Control of Coupled Spin Dynamics: Design of NMR Pulse Sequences by Gradient Ascent Algorithms. *Journal of Magnetic Resonance* **2005**, *172*, 296–305.
- (4) Lopez, C. J.; Lu, W.; Walls, J. D. Relaxation Selective Pulses in Fast Relaxing Systems. *J. Mag. Res.* **2014**, 242, 95–106.
- (5) Walls, J. D.; Marjanska, M.; Sakellariou, D.; Castiglione, F.; Pines, A. Selective excitation in dipole coupled systems. *Chem. Phys. Lett.* **2002**, *357*, 241–248.